Efficient Aerial Data Collection with Cooperative Trajectory Planning for Large-Scale Wireless Sensor Networks

Yuchao Zhu, *Student Member, IEEE*, and Shaowei Wang, *Senior Member, IEEE*

***Abstract*—Due to the flexibility and agility, unmanned aerial vehicle (UAV) is a promising way for gathering data generated by wireless sensor networks. However, the limited battery capacity of the UAV restricts its application on many occasions, e.g., the networks deployed in the wild. In this paper, we propose a cooperative trajectory planning scheme to deal with the energy issue of the UAV, where a truck carrying backup batteries moves along with the UAV acting as a "mobile recharging station". Our optimization task is to minimize the total mission time for gathering data from all the sensor nodes, which can be achieved by solving two problems: First, we need to divide the entire mission area into multiple subregions so that the UAV can hover over each subregion to collect the data of the sensor nodes through just one taking-off and landing under the constraint of battery capacity; second, we should find out the optimal trajectory of the truck so that the UAV can get to the hovering positions of each subregion from the truck and fly back to it before the battery drains considering the road condition in real world. We introduce an efficient clustering algorithm to partition the area into subregions in a load-balanced way to minimize the number of movements of the UAV. The trajectory planning task is formulated as a coordinated traveling salesman problem, which is solved by a three-step trajectory planning algorithm heuristically, and we also give the analysis of the upper bound and lower bound to demonstrate the performance guarantee. Numerical results show that our proposed scheme provides an effective and cost-efficient way for the data collection of large-scale wireless sensor networks in practical scenarios.**

***Index Terms*—Data collection, trajectory planning, unmanned aerial vehicles, wireless sensor network.**

I. Introduction

INTERNET of Things (IoT) is one of the indispensable technologies in the near future, in which everything is connected to the Internet, leading us to the realm of ubiquitous and intelligent wireless network [1]. The basic premise of the IoT is to widely deploy smart and dedicated sensor nodes (SNs) to collect and transmit data with only occasional human involvements, thus sharing information and further coordinating decisions. Wireless sensor network (WSN), where numerous low-cost, low-power, small-size SNs are spatially distributed for monitoring and recording ambient environment conditions [2], are widely deployed in diverse applications ranging from military scenarios to civil scenarios, such as intrusion detection [3], homeland security surveillance [4], volcano supervision [5], soil monitoring for smart agriculture [6], forest fire inspection [7].

With the explosive growth of the number of SNs deployed in the WSN, the data collection of these SNs becomes a critical and challenging task. Existing works can be generally categorized into three types according to the transmission approaches for data gathering from SNs to the data center, as shown in Fig. 1. Traditionally, the WSN is organized in a static manner, where the sensed data is collected and relayed via a multi-hop routing network to the destination (e.g., ground base station), as depicted in Fig. 1(a). The emphasis related to this scheme is on the routing design issue to find optimal forwarding routes [8]. Whereas, collecting a massive amount of data from widely or sparsely deployed SNs would cause the overuse of the relay nodes and the unreliable wireless links, which can lead to reduced network lifetime and degraded data transmission rates, respectively. Ground mobile sinks are thus introduced to overcome these problems. As illustrated in Fig. 1(b), one or more ground vehicles equipped with data sinks are employed for data collection [9], where the ground vehicle visits each SN directly or visits the SNs that are selected as relay nodes. Since the routing network is partially or fully replaced by the mobile sink, this approach can alleviate the transmission burden of SNs for relay [10]. Nevertheless, it is noteworthy that one of the distinguishing features of the aforementioned WSN application scenarios is that the SNs are usually distributed in the vast land. The deployment of terrestrial Internet infrastructures is difficult and expensive in these remote areas such as the wilderness and deep forests, posing an obstacle to data collection in a static manner. In addition, some areas are dangerous and hard-to-reach (e.g., volcano and swamp) for ground vehicles, increasing the difficulty for data collection.

Recently, with the ever-accelerating progress in design and production, unmanned aerial vehicle (UAV) has been foreseen as a key enabler in many domains. The applications of UAV can be generally summarized as ubiquitous coverage, relay and information dissemination/data collection [11]–[13]. Thanks to the agility and high maneuverability, UAVs can act as aerial mobile sinks to enable fast and reliable data collection in WSNs [14]. As illustrated in Fig. 1(c), the UAVs can fly towards the clusters of SNs and establish low power com-

Manuscript received May 17, 2021; revised September 1, 2021; accepted October 21, 2021. This work was partially supported by the National Natural Science Foundation of China under Grants 61931023 and U1936202. Part of this work has been accepted for presentation at IEEE Global Communications Conference, Madrid, Spain, December 7-11, 2021. The associate editor coordinating the review of this article and approving it for publication was M. Bennis. *(Corresponding author: Shaowei Wang.)*

The authors are with the School of Electronic Science and Engineering, Nanjing University, Nanjing 210023, China (e-mail: dz20230030@smail.nju.edu.cn; wangsw@nju.edu.cn).

This article has been accepted for publication in a future issue of this journal, but has not been fully edited. Content may change prior to final publication. Citation information: DOI 10.1109/TCOMM.2021.3124950, IEEE Transactions on Communications

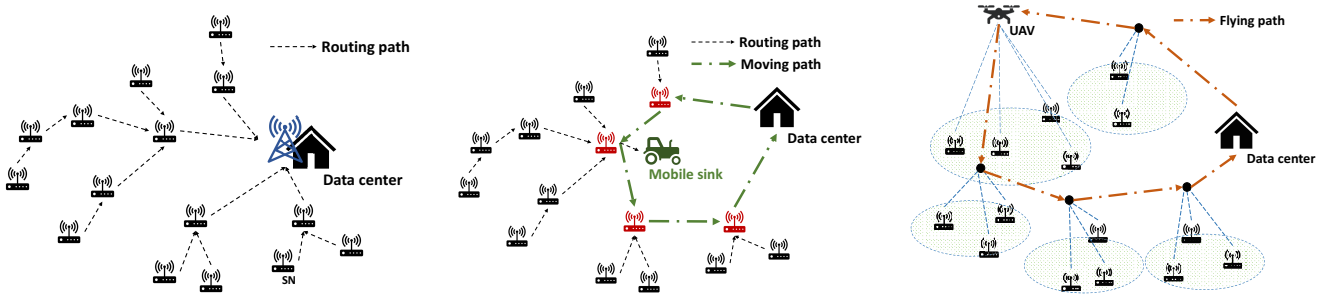

(a) Static sink (b) Ground mobile sink (c) Aerial mobile sink

Fig. 1. Three types of data collection in WSN.

munication links with the SNs [15], which is more efficient compared with road-restricted and low-speed ground mobile sinks. Moreover, by leveraging the line-of-sight dominated air-to-ground channels, UAVs can also provide high-quality data transmission [16]. In [17], the data gathering mission is abstracted as a traveling salesman problem (TSP)and solved by a fast path planning algorithm with division and combination. It shows good performance when SNs are deployed evenly. For the case of one UAV and one-dimensional WSN, [18] optimizes the time-varying UAV speed as well as the transmission interval to minimize the flight time of the UAV. In [19], the authors propose a unified scheme for age-optimal data collection, which optimizes the UAV hovering positions to minimize the SN's uploading time. A trajectory planning algorithm based on dynamic programming is also developed to minimize the UAV's flying time. In [20], an adaptive modulation scheme is adopted to improve the energy-efficiency of SNs while guaranteeing the fairness between different SN clusters. To avoid collision caused by simultaneous transmission from numerous SNs, a priority-based data access scheme with consideration of UAV's mobility is proposed in [21], which can improve the efficiency of transmission and prolong the lifetime of SNs. In the case that SNs have different and limited buffer sizes, a time-sensitive data collection mission to maximize the number of served SNs is studied in [22], where the UAV's trajectory and radio resource allocation are jointly optimized via a successive convex approximation algorithm. Considering a massive number of SNs, a two-tier UAV communication strategy is proposed in [23], where ground access points are introduced to help the transmission between the SNs and the UAV. In [24], a 3D trajectory optimization problem is studied to maximize the the minimum average data collection rate in a WSN under Rician fading channels.

However, the on-board energy, which is finite due to the size, weight and power of the aircraft, tends to be a fatal limitation that greatly influences the UAV's performance in practice [25]. With the development in supporting infrastructures, recent works envisage that the UAV's battery can be recharged or replaced whenever used up during its flight, which can be enabled by an automatic battery replacement system [26]. Given one fixed charging station, [27] studies energy-efficiency oriented scenario where multiple rechargeable UAVs are cooperatively dispatched to provide seamless and long-term coverage for ground IoT devices. The node assignment, UAVs' trajectory and transmit power control are jointly optimized by a block coordinate descent-based iterative algorithm, while only three IoT nodes are considered. In [28], the mission area is divided into multiple grids and wireless charging devices for the UAV are located at the center of each grid. Reinforcement learning is introduced to make the decisions of selecting the charging point, the flying height and the connected SN so as to improve the UAV's energy-efficiency. In [29], optimal placement of UAV charging stations is investigated, where the UAV's flying distance and the number of charging stations are jointly minimized. However, this scheme is lack of scalability and flexibility since the deployment of charging stations is fixed.

Fundamentally speaking, the energy issue is still a bottleneck of UAV-assisted WSNs from the viewpoint of system design, especially for large-scale WSNs. To this end, we try to endow the charging station with mobility so as to flexibly compensate for the battery capacity of the UAV. In this paper, on the basis of aerial data collection, we investigate a novel mobile sink approach to realize high-efficient periodic data collection for large-scale WSNs. The UAV, assisted by a truck carrying backup batteries, is dispatched to visit the clusters of SNs for data gathering, where the UAV acts as a mobile sink and the truck serves as a mobile battery swap station for the UAV. Our objective is to minimize the mission time of collecting data from all the SNs under the constraint of UAV's flight endurance, which can be fulfilled by solving two subproblems, i.e., optimal selection of hovering positions and optimal trajectory planning. First, a clustering method is introduced to partition the region of interest into multiple subregions that contain an approximately equal number of SNs based on the maximum coverage radius and capacity of the UAV, where the horizontal and vertical positions of the UAV are determined by the cluster centers and the subregion sizes, respectively. Second, we show that the trajectory design can be modeled as a combinatorial optimization task to find the sequence of visiting target subregions as well as the locations that the UAV and the truck rendezvous with each other, which is an extension of TSP. To our best knowledge, this is the first work that studies the UAV-aided data collection in WSNs with a "mobile recharging station" from a collaborative trajectory planning perspective [30]. Finally, we develop a heuristic three-step algorithm to solve the collaborative trajectory planning problem, and analyze the upper bound and

This article has been accepted for publication in a future issue of this journal, but has not been fully edited. Content may change prior to final publication. Citation information: DOI 10.1109/TCOMM.2021.3124950, IEEE Transactions on Communications

the lower bound of the algorithm. Numerical results verify that our proposal is effective and efficient, which can provide a guideline for the system design of data collection in real application scenarios.

The rest of the paper is organized as follows. Section II illustrates the data collection model and formulates the optimization task. In Section III, our proposed algorithm is given in detail, along with the analysis of the upper and lower bounds. Section IV provides numerical results and performance evaluation. Finally, Section V presents concluding remarks.

II. System Model And Problem Formulation

A. Network Description

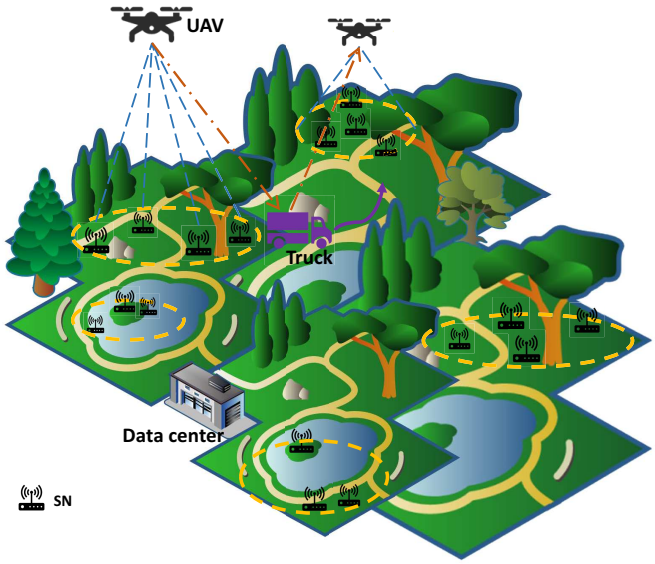

(a)

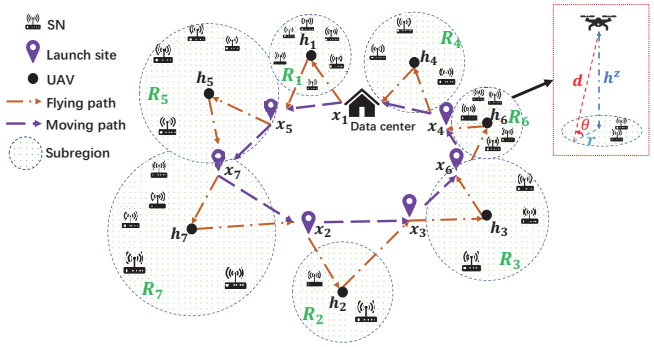

(b)

Fig. 2. Data collection of WSN in suburban environment.

Consider a WSN deployed in region $\mathcal{R} \in \mathbb{R}^2$, as depicted in Fig. 2(a), made up of a data center, a truck, a rotary-wing UAV and K SNs denoted by $\mathcal{K} = \{s_1, s_2, ..., s_K\}$. Suppose that each SN $s_k \in \mathcal{K}$ has a fixed location in the 3D Cartesian coordinate system, which is denoted as $\boldsymbol{z}_k = (s_k^x, s_k^y, 0)$. Since the UAV operates in hovering to gather the data from the clusters of SNs, the entire region is divided into n subregions so that the UAV can collect data from SNs in each subregion through one taking-off and landing. Due to the limited battery capacity of the UAV, a truck is dispatched to aid the UAV so that the UAV can fly back to the moving truck to replace its battery and then flies to the next subregion.

To illustrate the network model more clearly, we show the top view of Fig. 2(a) in Fig. 2(b). The set of subregions and UAV's 3D hovering positions are represented by $\mathcal{R}_s = \{R_1, R_2, ..., R_n\}$ and $\mathcal{H} = \{\boldsymbol{h}_1, \boldsymbol{h}_2, ..., \boldsymbol{h}_n\}$, respectively. When the UAV hovers at $\boldsymbol{h}_i = (h_i^x, h_i^y, h_i^z)$, it establishes communication links with the SNs located in subregion R_i, where the coverage radius of the UAV is related to its altitude. The amount of time required for collecting data from one SN is set as T_s, thus the hovering time above each subregion is proportional to the number of SNs in each subregion. Then the UAV flies back to the truck for battery replenishment before visiting the next subregion, the locations at which they rendezvous with each other are represented by "launch sites" $\mathcal{X} = \{\boldsymbol{x}_i = (x_i^x, x_i^y, 0), 1 \le i \le n\}$. Let $\mathcal{U} \ni \sigma(\cdot)$ denote the set of permutations of $\{1, 2, ..., n\}$ representing all the possible sequences of visiting subregions, where we set $\sigma(n+1) = \sigma(1)$ to simplify the notation (e.g., $\sigma = \{1, 5, 7, 2, 3, 6, 4, 1\}$ in Fig. 2(b)). Thus, the trajectories of the truck and the UAV can be represented as $[\boldsymbol{x}_{\sigma(1)}, \boldsymbol{x}_{\sigma(2)}, ..., \boldsymbol{x}_{\sigma(n+1)}]$ and $[\boldsymbol{x}_{\sigma(1)}, \boldsymbol{h}_{\sigma(1)}, \boldsymbol{x}_{\sigma(2)}, ..., \boldsymbol{h}_{\sigma(n)}, \boldsymbol{x}_{\sigma(n+1)}]$, respectively, where the data center is the start/end point.

B. Air-to-Ground Channel Model

For the UAV, the air-to-ground channel takes both line-of-sight (LoS) links and non-line-of-sight (NLoS) links into consideration, which is different from the ground-to-ground channel. The probability of LoS is dependent on the position of the UAV and SNs, geographic environments, density and height of buildings and so on, which can be closely approximated to a simple modified sigmoid function of the following form [16]:

$$P_{LoS}(\theta) = \frac{1}{1 + a\exp[-b(\theta - a)]}, \tag{1}$$

where a, b are parameters related to the environment, θ represents the elevation angle between the SNs and the UAV, which can be expressed as $\theta = \frac{180^\circ}{\pi}\arctan(h^z/r)$, where h^z is the hovering altitude of the UAV and r is the horizontal distance between the SNs and the UAV, as depicted in Fig. 2(b).

The path loss for the air-to-ground communication can be expressed as follows:

$$L_p = \left(\frac{4\pi f_c d}{c}\right)^2 \beta_p, \ p \in \{LoS, NLoS\}, \tag{2}$$

where c is the speed of light, f_c represents the carrier frequency and d represents the distance between the UAV and the ground SNs. β_{LoS} and β_{NLoS} refer to the excessive path loss of LoS and NLoS links, respectively.

Note that the probability of NLoS links is $P_{NLoS}(\theta) = 1 - P_{LoS}(\theta)$, so the average path loss model (in dB) can be

This article has been accepted for publication in a future issue of this journal, but has not been fully edited. Content may change prior to final publication. Citation information: DOI 10.1109/TCOMM.2021.3124950, IEEE Transactions on Communications

expressed as follows [31]:

$$\begin{aligned} L(h^z, r) &= \sum_p L_p P_p(\theta) \\ &= 20\log d + 20\log f_c + 20\log\Big(\frac{4\pi}{c}\Big) + P_{LoS}(\theta)\eta_{LoS} \\ &\quad + \big(1 - P_{LoS}(\theta)\big)\eta_{NLoS} \\ &= 20\log\sqrt{(h^z)^2 + r^2} \\ &\quad + \frac{A}{1 + a\exp\big[-b\big(\frac{180^\circ}{\pi}\arctan(\frac{h^z}{r}) - a\big)\big]} + B, \end{aligned} \tag{3}$$

where $\eta_{LoS} = 10\log\beta_{LoS}$, $\eta_{NLoS} = 10\log\beta_{NLoS}$. $A = \eta_{LoS} - \eta_{NLoS}$ and $B = 20\log f_c + 20\log(\frac{4\pi}{c}) + \eta_{NLoS}$ are constants under a given environment.

To guarantee the communication link between UAV and SNs, a threshold Γ is introduced to represent the maximum allowable path loss corresponding to the minimum transmission rate requirement of data collection. We assume that the SNs could establish connection with the UAV if $L(h^z, r) \leq \Gamma$, i.e., the UAV's maximal coverage radius can be mathematically expressed as $r_{max} = r|_{L(h^z,r)=\Gamma}$. Fig. 3 shows the variation

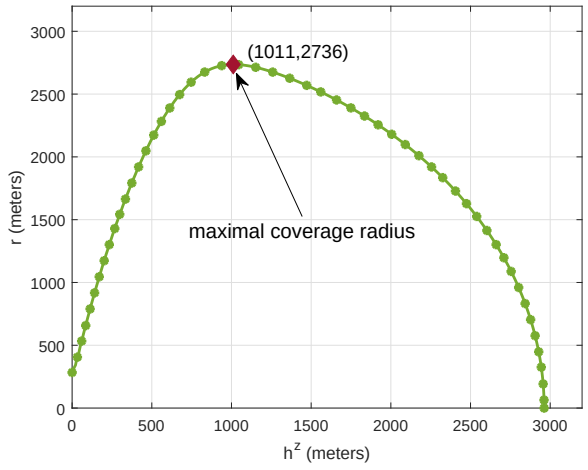

Fig. 3. Coverage radius r vs. UAV altitude h^z curve with $\Gamma = 108$ dB, in a suburban environment.

of coverage radius r with respect to UAV altitude h^z as per (3) for a suburban environment, where Γ is set as 108 dB. The coverage radius rises first and then descends as the altitude of the UAV increases, which indicates that h^z could be adjusted to achieve different coverage area while satisfying the same path loss requirement. The figure also shows the maximal coverage radius and corresponding UAV altitude by numerically solving $\partial r_{max}/\partial h^z = 0$, which gives a reference to the number of subregions need to be divided.

C. Energy Consumption Model for Rotary-Wing UAV

Generally speaking, the UAV's energy consumption is composed of communication related energy and propulsion energy. The former includes that for signal processing, signal radiation and reception, etc. Here we denote the communication-related power as constant P_c (in Watt) for simplicity.

TABLE I
NOTATIONS AND PHYSICAL MEANINGS OF VARIABLES IN POWER CONSUMPTION MODEL

Notation	Physical meaning
Ω	Blade angular velocity (in radians/second)
ρ	Air density (in kg/m^3)
A_r	Rotor disc area (in m^2)
d_0	Fuselage drag ratio
P_0	Blade profile power in hovering status (in Watt)
P_i	Induced power in hovering status (in Watt)
R	Rotor radius (in meter)
s	Rotor solidity (in m^3)
V_0	Mean rotor induced velocity in forwarding flight (in m/s)

The propulsion energy is consumed to keep the UAV aloft as well as support its movement, and the power consumption model of the UAV as a function of flying speed can be approximately expressed as follows [32], [33]:

$$P(v) = P_0\Big(1 + \frac{3v^2}{\Omega^2 R^2}\Big) + \frac{P_i V_0}{v} + \frac{1}{2}d_0\rho s A_r v^3, \tag{4}$$

where v is the velocity of the UAV. The notations and the corresponding physical meanings of the variables in (4) are clarified in Table I. Also note that, P_0 and P_i are two constants representing the blade profile power and induced power in hovering status, respectively, which depend on the weight of the UAV, air density, and rotor disc area, etc.

D. Problem Formulation

Considering a delay-tolerant data collection mission, we place emphasis on the amount of time needed to complete all the data collection. Denote $v_0, v_1 > 0$ as the speed of the truck and the UAV [1], respectively, with $v_0 < v_1$. The problem can be mathematically formulated as follows:

$$\begin{aligned} &\underset{\boldsymbol{x}_1,\ldots,\boldsymbol{x}_n,\sigma\in\mathcal{U}}{\text{minimize}} \sum_{i=1}^{n} \max\Big\{\frac{1}{v_0}||\boldsymbol{x}_{\sigma(i)} - \boldsymbol{x}_{\sigma(i+1)}||, \\ &\frac{1}{v_1}\big(||\boldsymbol{x}_{\sigma(i)} - \boldsymbol{h}_{\sigma(i)}|| + ||\boldsymbol{h}_{\sigma(i)} - \boldsymbol{x}_{\sigma(i+1)}||\big) + T_s N_{\sigma(i)}\Big\} \\ &\text{s.t.} \quad \frac{1}{v_1}E_f\big(||\boldsymbol{x}_{\sigma(i)} - \boldsymbol{h}_{\sigma(i)}|| + ||\boldsymbol{h}_{\sigma(i)} - \boldsymbol{x}_{\sigma(i+1)}||\big) \\ &\quad + E_h T_s N_{\sigma(i)} \leq E_{max}, \end{aligned} \tag{5}$$

where $N_{\sigma(i)}$ is the number of SNs in subregion $R_{\sigma(i)}$. E_f, E_h are the energy consumption of flying and hovering, respectively, and the total capacity of the battery is denoted as E_{max}. The UAV only establishes connection with ground SNs when it hovers above the corresponding subregions, so it can be derived that $E_f = P(v_1)$ and $E_h = P(0) + P_c$, respectively. The first term in $\max\{\cdot,\cdot\}$ represents the time needed for the truck to move from one launch site to the next, the second term corresponds to the amount of time for the UAV to fly away from one launch site, reach its hovering position and collect data from SNs, then return to meet the truck at the next launch site for battery replacement. The constraint guarantees that the UAV could fly back to the truck before its energy

[1]Uniform speed is considered for simplicity, which is reasonable for the scenario of large-scale WSN.

drains. Problem (5) is NP-hard since it is a generalization of TSP with the constraints of the rendezvous of the UAV and the truck and the battery capacity of the UAV.

III. Our Proposed Scheme

To address (5), we need to select the optimal hovering positions $\mathcal{H}$ at first, i.e., the following question should be answered: Given a region with unevenly distributed SNs, how can we divide the entire region into the minimum number of subregions while satisfying the constraints of UAV's capacity and achievable coverage radius? After determining the target hovering positions, we develop a three-step trajectory planning strategy to heuristically solve the coordinated trajectory optimization problem.

A. Selection of Hovering Positions

For preliminary preparation, we estimate the number of subregions to be divided, which relies on both the capacity and the coverage range of the UAV. Considering the capacity requirement, the number of subregions is $n_s = \left\lceil \frac{K}{k_m} \right\rceil$, where k_m is the maximum number of SNs that the UAV can serve considering battery capacity. Considering the coverage constraint, the number of subregions is $n_c = \left\lceil \frac{A}{\pi r_{max}^2} \right\rceil$, where A denotes the area of region $\mathcal{R}$, and the coverage of the UAV is considered as a circle. Then, the approximate number of divided subregions is denoted as:

$$n = \max\{n_s, n_c\}. \tag{6}$$

Note that the number of subregions would be minimal when the SNs are equally assigned between the subregions. Thus, we try to partition the mission area into at least n subregions in a load-balanced way. Since the distribution of desired hovering positions of the UAV is related to the density of SNs, we introduce a clustering method called ISODATA to determine $\mathcal{H}$ [34]. The SNs are grouped together if they are closest to the centroid of a cluster.

The clustering procedure is shown in Algorithm 1, the parameters of which include follows:

- I_{max}: maximum number of iterations
- n_e: expected number of clusters
- N_{min}: minimum size of clusters
- d_{min}: minimum distance between two cluster centroids
- ϵ_{max}: allowed standard deviation of each cluster

First, select K_c samples randomly from the input dataset as the initial centers, the corresponding clusters of which is denoted by $C_1, C_2, ..., C_{K_c}$. Then each SN would be assigned to the closest cluster center, which can be mathematically written as:

$$C_i = \{s \in \mathcal{K} |\ ||s - c_i|| \leq ||s - c_j||,\ \forall i \neq j\}. \tag{7}$$

A discarding procedure is introduced to remove the clusters that possess SNs fewer than the given threshold, i.e., when $|C_i| \leq N_{min}$, the cluster C_i would be discarded along with reducing the number of clusters. The centers of clusters are updated by:

$$c_i = \frac{1}{|C_i|} \sum_{s \in C_i} s, \tag{8}$$

Algorithm 1 Clustering by ISODATA

Initialization: set parameters I_{max}, n_e, N_{min}, d_{min}, ϵ_{max} and input the set of SNs $\mathcal{K}$;
Select K_c samples randomly from $\mathcal{K}$ as the initial cluster centers $\{c_1, ..., c_{K_c}\}$;
$I = 0$;
repeat
  $I = I + 1$;
  assign SNs into clusters by Eq. (7);
  for $j = 1 : K_c$ **do**
    if $|C_j| \leq N_{min}$ **then**
      $K_c = n_e - 1$;
      assign SNs into clusters by Eq. (7);
    end if
  end for
  Update cluster centers by Eq. (8);
  if $K_c < n_e/2$ **then**
    Split procedure:
    calculate the standard deviation of each cluster $\{\epsilon_1, \epsilon_2, ..., \epsilon_{K_c}\}$;
    $\epsilon_l = \max\{\epsilon_1, \epsilon_2, ...\epsilon_{K_c}\}$;
    if $\epsilon_l > \epsilon_{max}$ & $|C_l| \geq 2N_{min}$ **then**
      split the cluster into two clusters;
      $n_e = n_e + 1$;
      Update cluster centers by Eq. (9);
    end if
    return to step 4;
  end if
  if $K_c > 2n_e$ || $I\ mod\ 2 == 0$ **then**
    Merge procedure:
    calculate the distance between all the cluster centers and record in matrix D_{dis};
    if $D_{dis}(i,j) < d_{min}$ **then**
      merge the two clusters C_i and C_j as one cluster;
      Update cluster center by Eq. (10);
      $n_e = n_e - 1$;
    end if
  end if
until $I = I_{max}$;
return The cluster centers c.

We explain the split and merge operations in detail. In the split procedure, the standard deviation of each cluster is calculated, and the maximum one is picked up and denoted as ϵ_l. If $\epsilon_l > \epsilon_{max}$ and the number of SNs in this cluster C_l is not smaller than $2N_{min}$, the split operation would be triggered. In the merge procedure, calculate the distance between all the cluster centers, denoted as matrix D_{dis}, with $D_{dis}(i,i) = 0$. If $D_{dis}(i,j) < d_{min}$, the merge operation would be triggered. The update rules of cluster centers are as follows:

$$c_i^+ = c_i + \epsilon_l,\ c_i^- = c_i - \epsilon_l, \tag{9}$$

$$c_{new} = \frac{1}{|C_i| + |C_j|}(|C_i|c_i + |C_j|c_j), \tag{10}$$

which correspond to the split and merge operation, respectively.

This article has been accepted for publication in a future issue of this journal, but has not been fully edited. Content may change prior to final publication. Citation information: DOI 10.1109/TCOMM.2021.3124950, IEEE Transactions on Communications

By split and merge, ISODATA can find the appropriate clusters efficiently. We use SN set $\mathcal{K}$ as the input and the expected number of clusters is set as n, the output centroids are the horizontal part of the hovering positions $\mathcal{H}$ of the UAV. Then, as the clusters/subregions have diverse shapes and sizes, we adjust the altitude of the UAV to achieve different coverage radiuses. The required coverage radius of the UAV above subregion R_i is $r_i = \max_k\{||(h_i^x, h_i^y, 0) - \boldsymbol{z}_k||,\ s_k \in R_i\}$, which is determined by the SNs at the edge. The corresponding altitude h_i^z of the UAV can be calculated by $L(h_i^z, r_i) = \Gamma$.

B. Optimal Trajectory Planning

The trajectory planning is to jointly optimize the routes of the UAV and the truck given target hovering positions, the key point of which lies in finding the optimal locations of launch site. We propose an efficient algorithm to address the optimization task defined by (5) considering the fact that (5) over variables $\boldsymbol{x}_i$ will be convex under a fixed permutation σ, which falls into a second-order cone program problem. The details are given in Algorithm 2 and summarized as follows:

Step 1: Initialize the order of visiting all the target hovering positions $\mathcal{H}$.

We set the initial sequence of $\{\boldsymbol{h}_1, ..., \boldsymbol{h}_n\}$ the same as their optimal TSP tour. The methods to solve TSP are diverse, such as ant colony algorithm [35], simulated annealing [36]. Lin-Kernighan heuristic (LKH), first proposed in [37], is an efficient method for solving TSP. We use an LKH solver constructed in [38] to find a promising TSP solution and initialize the visiting sequence σ.

Step 2: Solve problem (5) with fixed σ.

Given one permutation σ to visit all the subregions, (5) can be rewritten as follows:

$$\begin{aligned}
&\underset{\boldsymbol{x}_1,...,\boldsymbol{x}_{n+1},t_1,...,t_{n+1}}{\text{minimize}} \quad t_{n+1} \\
\text{s.t. } C_1:\ & t_i \geq t_{i-1} + \frac{1}{v_1}\big(||\boldsymbol{x}_{i-1} - \boldsymbol{h}_{i-1}|| + ||\boldsymbol{h}_{i-1} - \boldsymbol{x}_i||\big) \\
& \quad + T_s N_{i-1},\ \forall i \in \{2, ..., n+1\}, \\
C_2:\ & t_i \geq t_{i-1} + \frac{1}{v_0}||\boldsymbol{x}_{i-1} - \boldsymbol{x}_i||,\ \forall i \in \{2, ..., n+1\}, \\
C_3:\ & ||\boldsymbol{x}_{i-1} - \boldsymbol{h}_{i-1}|| + ||\boldsymbol{h}_{i-1} - \boldsymbol{x}_i|| \\
& \quad \leq v_1 \frac{E_{max} - E_h T_s N_{i-1}}{E_f},\ \forall i \in \{2, ..., n+1\}, \\
C_4:\ & t_1 = 0, \\
C_5:\ & \boldsymbol{x}_1 = \boldsymbol{x}_{n+1},
\end{aligned} \tag{11}$$

where $t_{(\cdot)}$ represents the accumulative time at each ordered point. $\boldsymbol{x}_1 = \boldsymbol{x}_{n+1}$ is the data center with fixed location, where the UAV and the truck start their tours and finally return. We can solve this convex optimization problem by using standard techniques such as CVX [39], then the optimal coordinated routes under ordered visiting assignment can be found.

Step 3: Explore new visiting sequences.

It is noteworthy that the optimal σ of the coordinated tour is not necessarily the same as that induced by the TSP tour, thus we apply 2-OPT exchanges to explore new possible permutations, and Step 2 is repeated under new visiting order for every exchange. Step 3 will stop when no additional improvements can be achieved.

Algorithm 2 Three-step coordinated trajectory planning

Input: Mission region $\mathcal{R}$, hovering positions $\mathcal{H}$, parameters of truck and UAV: $v_0, v_1, E_f, E_h, E_{max}, T_s$, and the maximum number of iteration I_m.
Step 1: Using LKH algorithm to solve the TSP tour of $\mathcal{H}$ to initialize the visiting sequence;
Return the solution σ;
Step 2: Using CVX to solve (11) with σ to find the initial optimal routes;
Return $\sigma^{new} \leftarrow \sigma$, $t_{n+1}^{new} \leftarrow t_{n+1}$, $\boldsymbol{x}^{new} \leftarrow \boldsymbol{x}$;
Step 3: Using 2-OPT to explore new routes:
$i = 1$;
while $i < I_m$ **do**
  2-OPT exchange;
  Return new σ;
  Solve problem (11) with σ;
  if $t_{n+1} < t_{n+1}^{new}$ **then**
    $\sigma^{new} \leftarrow \sigma$, $t_{n+1}^{new} \leftarrow t_{n+1}$, $\boldsymbol{x}^{new} \leftarrow \boldsymbol{x}$;
  else
    σ^{new}, t_{n+1}^{new}, $\boldsymbol{x}^{new}$ do not change;
  end if
  $i \leftarrow i + 1$;
end while
Output: σ^{new}, $\boldsymbol{x}^{new}$, t_{n+1}^{new}.

C. Proof of bounds

The lower and upper bounds of (5) can be proved based on the continuous approximation analysis. Note that weakening the constraint would expand the solution space, which will not influence the bounds of the problem although the bounds may not be tight. So we set the constraint of the problem aside to obtain crude lower bound and upper bound for proof convenience. At first, we introduce a theorem given by [40], which describes the relationship of the average distance between a point sampled from $g(x)$ and a loop L. For notation convenience, let $d(x, L) = \min_{x' \in L} ||x - x'||$ denotes the distance between a point x and the loop L.

Theorem 1.[2] *Denote $\mathcal{D}$ as a compact planar region and let g be an absolutely continuous probability density function defined on $\mathcal{D}$. Let OPT(l) denoted the optimal objective value to the problem*

$$\begin{aligned}
\underset{L}{\text{minimize}} \quad & \iint_{\mathcal{D}} g(x) d(x, L) dx \\
s.t. \quad & \text{length}(L) = l,
\end{aligned} \tag{12}$$

where the optimization variable L is taken over the set of all loops in $\mathcal{D}$ whose length is well defined. Then

$$OPT(l) \sim \frac{1}{4l}\Big(\iint_{\mathcal{D}} \sqrt{g(x)} dx\Big)^2 \tag{13}$$

as $l \to \infty$.

[2]The proof can be found in detail in [40].

1) Lower bound: Denote $\boldsymbol{h}^p_{\sigma(i)} = (h^x_{\sigma(i)}, h^y_{\sigma(i)}, 0)$ as the projection of $\boldsymbol{h}_{\sigma(i)}$ on the 2D region plane $\mathcal{R}$. Refer to Fig. 2(b), it can be observed that for each $\boldsymbol{h}_{\sigma(i)}$, we can always find a $\boldsymbol{x}^{'}_{\sigma(i)}$ that is closest to $\boldsymbol{h}^p_{\sigma(i)}$ on the line segment $\overline{\boldsymbol{x}_{\sigma(i)}\boldsymbol{x}_{\sigma(i+1)}}$ of the truck route. Thus, according to the geometrical relationship, it is straightforward that the formula below always holds:

$$||\boldsymbol{x}_{\sigma(i)} - \boldsymbol{h}^p_{\sigma(i)}|| + ||\boldsymbol{h}^p_{\sigma(i)} - \boldsymbol{x}_{\sigma(i+1)}|| \geq 2||\boldsymbol{x}^{'}_{\sigma(i)} - \boldsymbol{h}^p_{\sigma(i)}||. \tag{14}$$

Denote $T_{\sigma(i)} = T_s N_{\sigma(i)}$, then the objective function of (5) satisfies:

$$\begin{aligned}
&\sum_{i=1}^{n} \max\Big\{\frac{1}{v_0}||\boldsymbol{x}_{\sigma(i)} - \boldsymbol{x}_{\sigma(i+1)}||, \\
&\quad \frac{1}{v_1}\big(||\boldsymbol{x}_{\sigma(i)} - \boldsymbol{h}_{\sigma(i)}|| + ||\boldsymbol{h}_{\sigma(i)} - \boldsymbol{x}_{\sigma(i+1)}||\big) + T_{\sigma(i)}\Big\} \\
&\geq \sum_{i=1}^{n} \max\Big\{\frac{1}{v_0}||\boldsymbol{x}_{\sigma(i)} - \boldsymbol{x}_{\sigma(i+1)}||, \\
&\quad \frac{1}{v_1}\big(||\boldsymbol{x}_{\sigma(i)} - \boldsymbol{h}^p_{\sigma(i)}|| + ||\boldsymbol{h}^p_{\sigma(i)} - \boldsymbol{x}_{\sigma(i+1)}||\big) + T_{\sigma(i)}\Big\} \\
&\geq \sum_{i=1}^{n} \max\Big\{\frac{1}{v_0}||\boldsymbol{x}_{\sigma(i)} - \boldsymbol{x}_{\sigma(i+1)}||, \frac{2}{v_1}d(\boldsymbol{h}^p_{\sigma(i)}, L) + T_{\sigma(i)}\Big\} \\
&\geq \max\Big\{\sum_{i=1}^{n}\frac{1}{v_0}||\boldsymbol{x}_{\sigma(i)} - \boldsymbol{x}_{\sigma(i+1)}||, \\
&\quad \sum_{i=1}^{n}\big(\frac{2}{v_1}d(\boldsymbol{h}^p_{\sigma(i)}, L) + T_{\sigma(i)}\big)\Big\} \\
&= \max\Big\{\frac{1}{v_0}\text{length}(L), \frac{2}{v_1}\sum_{i=1}^{n} d(\boldsymbol{h}^p_{\sigma(i)}, L) + KT_s\Big\},
\end{aligned} \tag{15}$$

where L here is regarded as the moving route of truck.

Then the lower bound of problem (5) can be expressed by the optimal objective value of problem (16):

$$\underset{L}{\text{minimize}}\ \max\Big\{\frac{1}{v_0}\text{length}(L), \frac{2}{v_1}\sum_{i=1}^{n} d(\boldsymbol{h}^p_{\sigma(i)}, L) + KT_s\Big\}. \tag{16}$$

Eq. (16) is still a combinatorial optimization problem, whose optimal value is hard to compute. As is standard in the continuous approximation paradigm, it is assumed that the projection of hovering positions $\boldsymbol{h}^p_{\sigma(i)}$ are independent samples from an absolutely continuous probability density function $g(\cdot)$ defined on $\mathcal{R}$. Based on the continuous approximation paradigm, the summation in (15) can be written as an integral over $\mathcal{R}$, which is given as follows:

$$\underset{L}{\text{minimize}}\ \max\Big\{\frac{1}{v_0}\text{length}(L), \frac{2n}{v_1}\iint_{\mathcal{R}} g(x)d(x, L)dx + KT_s\Big\}. \tag{17}$$

According to (13) of **Theorem 1**, problem (17) can be transformed into:

$$\underset{l\geq 0}{\text{minimize}}\quad \max\Big\{\frac{l}{v_0}, \frac{n}{2v_1 l}\big(\iint_{\mathcal{R}}\sqrt{g(x)}dx\big)^2 + KT_s\Big\}. \tag{18}$$

Obviously, the solution is given by:

$$l^* = \frac{KT_s v_0 + \sqrt{(KT_s v_0)^2 + 2nv_0/v_1(\iint_{\mathcal{R}}\sqrt{g(x)}dx)^2}}{2}, \tag{19}$$

and the optimal objective value can be calculated by:

$$opt(l^*) = \frac{KT_s + \sqrt{(KT_s)^2 + 2n/(v_0 v_1)(\iint_{\mathcal{R}}\sqrt{g(x)}dx)^2}}{2}. \tag{20}$$

2) Upper bound: Intuitively, it would take the most time to complete the mission when one is subject to an additional constraint that the truck keeps stationary whenever the UAV flies away to collect data. So we can obtain an upper bound by replacing the $\max\{\cdot,\cdot\}$ in (5) with a summation:

$$\begin{aligned}
&\sum_{i=1}^{n} \max\Big\{\frac{1}{v_0}||\boldsymbol{x}_{\sigma(i)} - \boldsymbol{x}_{\sigma(i+1)}||, \\
&\quad \frac{1}{v_1}\big(||\boldsymbol{x}_{\sigma(i)} - \boldsymbol{h}_{\sigma(i)}|| + ||\boldsymbol{h}_{\sigma(i)} - \boldsymbol{x}_{\sigma(i+1)}||\big) + T_{\sigma(i)}\Big\} \\
&\leq \sum_{i=1}^{n}\big(\frac{1}{v_0}||\boldsymbol{x}_{\sigma(i)} - \boldsymbol{x}_{\sigma(i+1)}|| + \frac{2}{v_1}||\boldsymbol{h}_{\sigma(i)} - \boldsymbol{x}^{'}_{\sigma(i)}|| + T_{\sigma(i)}\big) \\
&\leq \frac{1}{v_0}\text{length}(L) + \sum_{i=1}^{n}\Big(\frac{2}{v_1}\big(d(\boldsymbol{h}^p_{\sigma(i)}, L) + h^z_{\sigma(i)}\big) + T_{\sigma(i)}\Big) \\
&= \frac{1}{v_0}\text{length}(L) + \frac{2}{v_1}\sum_{i=1}^{n} d(\boldsymbol{h}^p_{\sigma(i)}, L) + \frac{2}{v_1}H + KT_s,
\end{aligned} \tag{21}$$

where $H = \sum_{i=1}^{n} h^z_{\sigma(i)}$ is a constant when given hovering positions.

Similar to the lower bound, the optimal objective value of problem (22) is the upper bound of problem (5):

$$\underset{L}{\text{minimize}}\ \frac{1}{v_0}\text{length}(L) + \frac{2}{v_1}\sum_{i=1}^{n} d(\boldsymbol{h}^p_{\sigma(i)}, L) + \frac{2H}{v_1} + KT_s, \tag{22}$$

whose continuous approximation can be written as follows:

$$\begin{aligned}
\underset{L}{\text{minimize}}\ &\frac{1}{v_0}\text{length}(L) + \frac{2}{v_1}\iint_{\mathcal{R}} g(x)d(x, L)dx \\
&+ \frac{2H}{v_1} + KT_s.
\end{aligned} \tag{23}$$

It is easy to see by applying **Theorem 1** again that (23) is asymptotically equivalent to:

$$\underset{l\geq 0}{\text{minimize}}\ \max\Big\{\frac{l}{v_0} + \frac{n}{2v_1 l}\big(\iint_{\mathcal{R}}\sqrt{g(x)}dx\big)^2 + \frac{2H}{v_1} + KT_s\Big\}, \tag{24}$$

whose optimal solution is given by:

$$l^* = \sqrt{\frac{nv_0}{2v_1}}\iint_{\mathcal{R}}\sqrt{g(x)}dx, \tag{25}$$

and the corresponding objective value is:

$$opt(l^*) = \sqrt{\frac{2n}{v_0 v_1}}\iint_{\mathcal{R}}\sqrt{g(x)}dx + \frac{2H}{v_1} + KT_s. \tag{26}$$

This article has been accepted for publication in a future issue of this journal, but has not been fully edited. Content may change prior to final publication. Citation information: DOI 10.1109/TCOMM.2021.3124950, IEEE Transactions on Communications

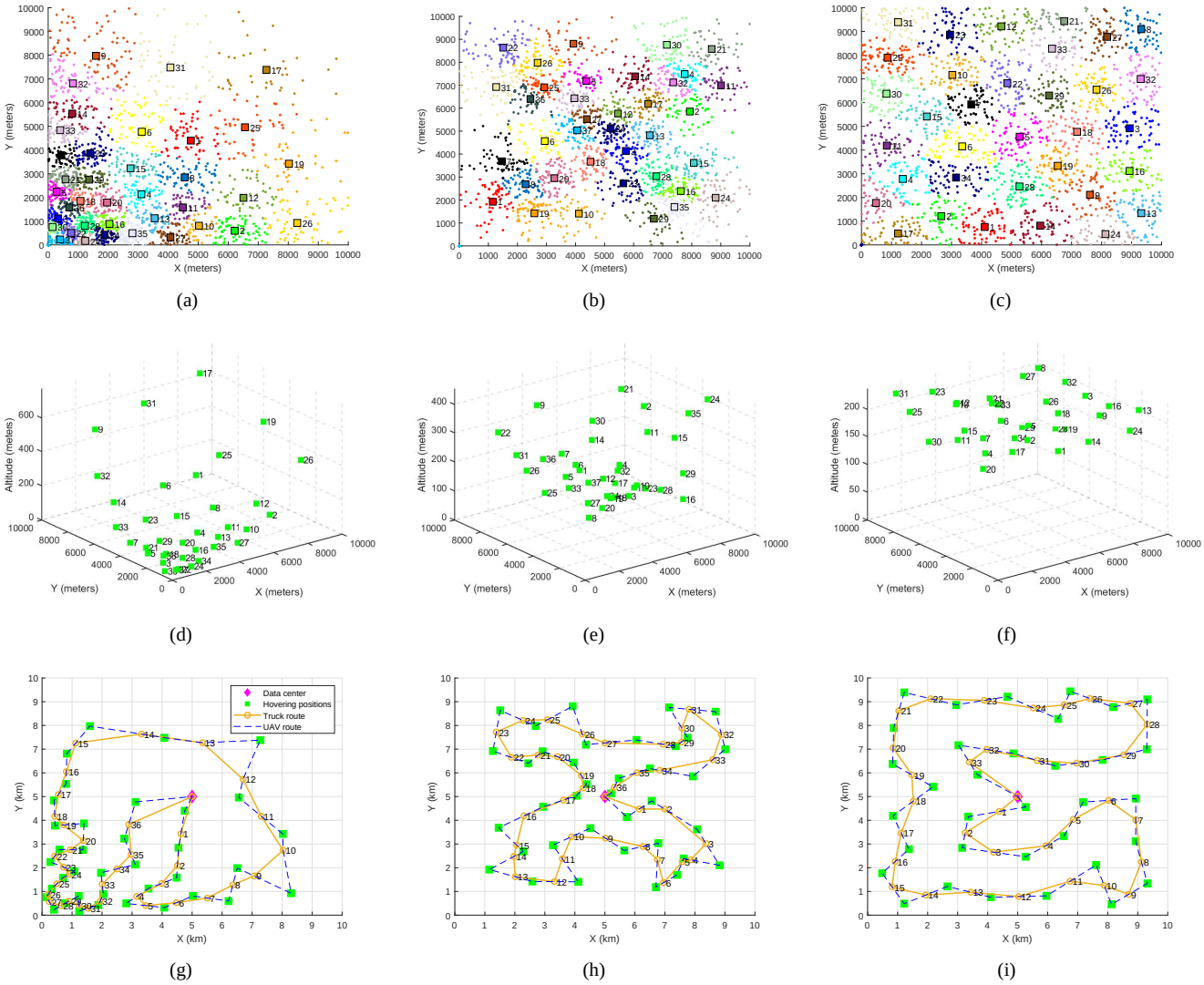

Fig. 4. The planning results for different distributions of SNs. (a)-(c) show the clustering results, where the dots and the squares in different colors represent SNs and the cluster centers, respectively. (d)-(f) show the adjusted altitudes of the UAV, the green squares represent the UAV's 3D hovering positions. (g)-(i) depict the trajectory design results, where the location of data center is denoted by a magenta diamond, the green squares represent the projection of UAV's hovering positions, the yellow circles represent the locations of launch site, the trajectories of the truck and the UAV are represented by yellow solid line and blue dash line, respectively.

IV. Numerical Results

We consider a geographical region in suburban of size 10×10 km^2, where 2000 SNs are deployed and the data center is located at the center of the area. The parameters in suburban environment with $f_c = 2$ GHz are $a = 4.88$, $b = 0.43$, $\eta_{LoS} = 0.1$, $\eta_{NLoS} = 21$, respectively [31]. The threshold of allowable path loss is set as $\Gamma = 108$ dB. The UAV's propulsion energy parameters are $\Omega = 300$ radians/s, $\rho = 1.225$ kg/m^3, $A_r = 0.503$ m^2, $d_0 = 0.3$, $R = 0.4$ m, $s = 0.05$, $V_0 = 4.03$ m/s, $P_0 = 79.86$ W, $P_i = 88.63$ W, respectively [33]. The communication-related power consumption is set as $P_c = 30$ W. The battery capacity of the UAV is 40 Wh. Note that, while the UAV's trajectories are naturally measured in Euclidean sense, the paths of the truck are non-Euclidean distance since the roads in reality are full of twists and turns, which introduces difficulty in measurement. However, since our emphasis is on the total time required to complete data collection, we can use an "equivalent speed" to compensate for the heterogeneous roads. Assume that the real road distance and Euclidean distance between one launch site and the next are l_r and l_e, respectively, and $l_r \geq l_e$. Let $v_0^{'}$ denote the speed of the truck on the real road. Then the time required for the truck to finish this piece of tour can be written as $t_r = l_r/v_0^{'}$ and $t_e = l_e/v_0$, respectively. It can be drawn that $t_r = t_e$ if we set $v_0 = \frac{l_e}{l_r} v_0^{'}$, and it is easy to see that $v_0 \leq v_0^{'}$. In other words, we can set a relatively small v_0 when using Euclidean distance to achieve the same result as if the truck moves at higher speed on real roads, which will not influence the total time to complete the tour. In short, unless otherwise specified, the speeds of truck and UAV are set as $v_0 = 20$ km/h and $v_1 = 80$ km/h, respectively.

First, we show the performance of our proposed scheme when given different distributions of SNs, as depicted in Fig. 4, where SNs in Fig. 4(a) and 4(b) are unevenly distributed,

This article has been accepted for publication in a future issue of this journal, but has not been fully edited. Content may change prior to final publication. Citation information: DOI 10.1109/TCOMM.2021.3124950, IEEE Transactions on Communications

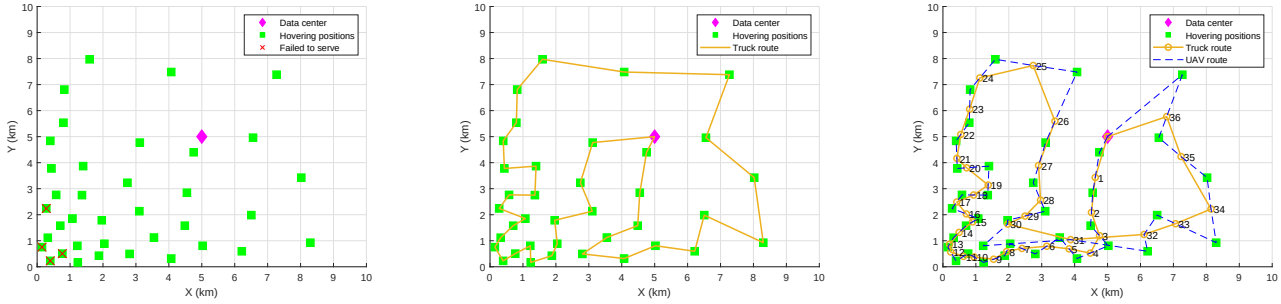

(a) (b) (c)

Fig. 5. (a) Single UAV flies forth and back between data center and all the subregions. (b) A truck following a TSP route carries a UAV to each hovering positions, and then the UAV flies vertically to the desired altitude for data collection. (c) Greedy-based coordinated trajectory planning.

SNs in Fig. 4(c) are uniformly deployed. For preliminary preparation, we first partition the mission region into multiple subregions with approximately equal load. Recall Fig. 3, we can obtain that the maximum achievable coverage radius of UAV is 2736 meters, then the estimated number of subregions that need to be divided is $n = 34$ according to (6), where k_m is set as 60 to reserve a margin. Thus, for the clustering method, parameters are set as $I_{max} = 100$, $n_e = 34$, $N_{min} = 35$, $d_{min} = 1$, $\epsilon_{max} = 1$, respectively. As shown in Fig. 4(a)-4(c), the corresponding number of clusters are 37, 37 and 34, respectively. Then, based on the size of subregions, we adjust the altitude of the UAV to cover all the SNs in each cluster. The UAV's 3D hovering positions of Fig. 4(a)-4(c) are given in Fig. 4(d)-4(f), which indicate that the UAV will decrease its hovering altitude when the density of SNs increases. Finally, the trajectory design results are illustrated in Fig. 4(g)-4(i).

Then, we compare our proposal with the following three methods: UAV-alone, truck-direct and greedy-based coordinated trajectory planning (Greedy). UAV-alone uses a UAV itself to fly forth and back between the fixed data center and all the subregions, where the data center also acts as a battery swapping station. Truck-direct uses a truck to directly carry a UAV to each subregion, where the truck follows a TSP route, then the UAV lifts off to the desired altitude for data collection and lands on the truck for battery replacement, this corresponds to setting $\boldsymbol{x}_{\sigma(i)} = \boldsymbol{h}_{\sigma(i)}$ for all i in our upper bound formulation. Greedy is an intuitive trajectory planning method in which the UAV always chooses the nearest one of the remaining hovering positions as its next target.

Taking the distribution of SNs in Fig. 4(a) as an example, we show the planning results of the UAV-alone, truck-direct and Greedy method in Fig. 5(a)-5(c), respectively. As can be seen, the UAV itself fails to visit all the subregions, it could only serve 33 subregions of total 37 subregions due to the limited battery capacity. It is obvious that such a problem would be severer as the size of the region becomes larger. For the truck-direct method, although it can complete the mission, the truck needs to take a longer path as compared to the route shown in Fig. 4(g) and the flexibility and agility of the UAV are not well exploited. For the Greedy method, the visiting sequence is slightly different from our proposal, and the routes of the UAV and truck are longer than those of our proposal since there exists crossovers and overlaps.

Other meaningful evaluation indexes are also employed to measure the performance. First, denote ω as the percentage of collected subregions, which indicates the feasibility of the methods. Then, let D_T and D_U denote the total traveling distance of the truck and the UAV, respectively [3]. ϕ represents the ratio of time paid for data collection to the total mission time, which indicates the efficiency of data collection. T_{total} is the completion time of the mission.

Table II gives the performance indexes under different distributions of SNs. For the UAV-alone method, there always exists subregions located in remote areas which are beyond the endurance of the UAV. Especially when the data center is far away from the subregions, the percentage of collected subregions is relatively low, which validates the infeasibility of this method in practice. For the truck-direct method, it is generally feasible in most road-unrestricted scenarios [4]. However, the efficiency is much lower than our proposal since our scheme can save 36.71% time in average. The reason is that the truck keeps stationary whenever the UAV leaves it for data collection in truck-direct method, which wastes time on waiting. While in our proposal, the truck takes a shorter path since the speed of the UAV is faster than the truck's and it could catch up with the moving truck. For the Greedy method, it outperforms the former two methods as the trajectories of the UAV and the truck are jointly considered. However, its total completion time is longer and its efficiency is lower as compared to our proposal. This is because Greedy could not find the optimal route.

We also investigate the system performance as a function of the number of SNs in Fig. 6 [5]. Fig. 6(a) shows that the total completion time is approximately proportional to the number of SNs, which is reasonable since the time spent for data collection increases along with the SNs. We can also see that our proposal consumes less time than the other two methods, about 3.28% and 35.64% time on average can be saved as compared to Greedy and truck-direct, respectively. Moreover, the gap becomes larger as the number of SNs grows. Fig. 6(b)

[3]Note that D_U of truck-direct method is calculated as the distance for taking-off and landing.

[4]It is worth mentioning that the method would also fail when the hovering positions, e.g., over the swamps, are unreachable for the ground vehicles.

[5]The performance of UAV-alone is not plotted here since it is infeasible.

This article has been accepted for publication in a future issue of this journal, but has not been fully edited. Content may change prior to final publication. Citation information: DOI 10.1109/TCOMM.2021.3124950, IEEE Transactions on Communications

TABLE II
EVALUATION INDEXES

SN distribution	Method	ω (%)	D_U (km)	D_T (km)	ϕ (%)	T_{total} (hour)
Fig. 4(a)	UAV-alone	89.19	272.49	0	47.84	Failed
	Truck-direct	100	7.37	45.93	53.76	5.17
	Greedy	100	53.55	38.49	80.58	3.44
	Our proposal	100	48.72	36.33	82.02	3.38
Fig. 4(b)	UAV-alone	94.59	219.47	0	52.20	Failed
	Truck-direct	100	10.40	52.55	50.18	5.54
	Greedy	100	68.88	45.65	76.34	3.64
	Our proposal	100	51.84	37.74	79.57	3.49
Fig. 4(c)	UAV-alone	91.19	229.14	0	51.82	Failed
	Truck-direct	100	6.66	56.69	48.77	5.69
	Greedy	100	75.03	54.25	74.76	3.72
	Our proposal	100	58.29	46.60	79.22	3.50

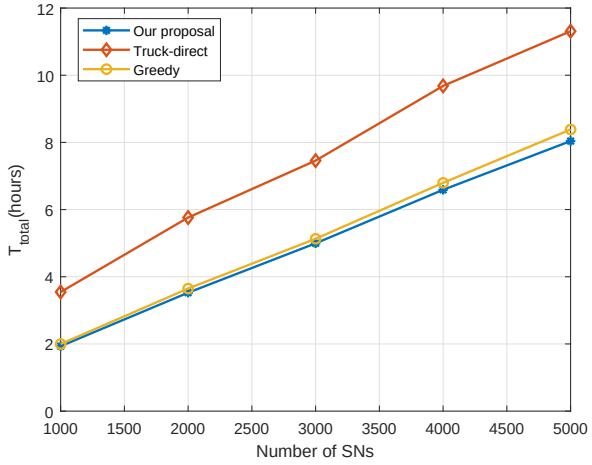

(a) The total completion time of data collection as a function of the number of SNs.

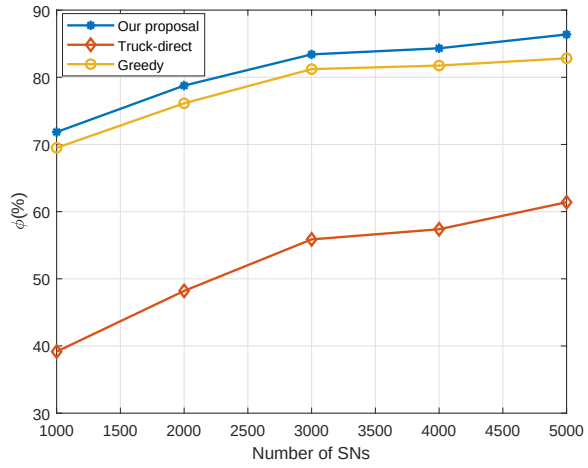

(b) The efficiency of data collection as a function of the number of SNs.

Fig. 6. The influence of the number of SNs, where SNs are uniformly distributed in a region of size 10×10 km^2.

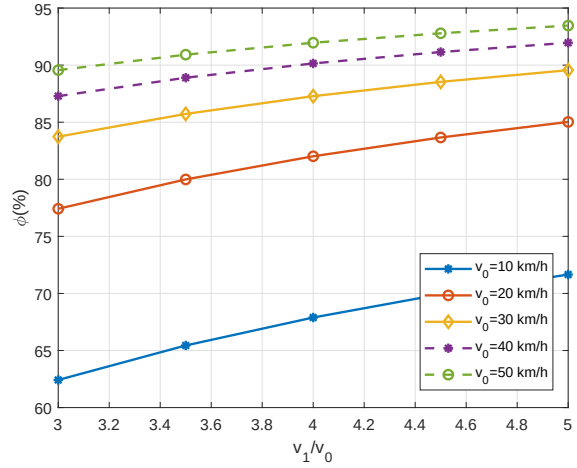

(a) The efficiency of data collection as a function of v_1/v_0.

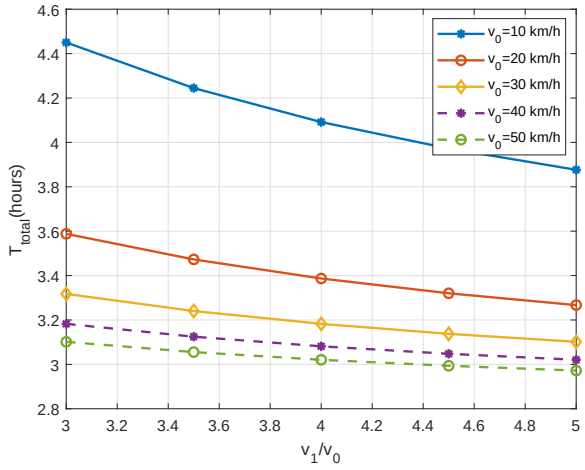

(b) The total completion time of data collection as a function of v_1/v_0.

Fig. 7. The influence of v_0 and v_1, based on the hovering positions shown in Fig. 4(d).

shows that the collection efficiency would also increase along with the number of SNs, this is because the increment of time required for data collection is much more than that of time required for moving when the density of SNs increases. It can also be observed that the collection efficiency of our proposal is higher than the other two methods. We can conclude from Fig. 6 that our proposal is high-efficient, and the gain is remarkable when the number of SNs is large.

Finally, we investigate the influence of the UAV and truck speed. In Fig. 7, we can see that the efficiency is approximately proportional to the ratio of the UAV's speed to the truck's, and

This article has been accepted for publication in a future issue of this journal, but has not been fully edited. Content may change prior to final publication. Citation information: DOI 10.1109/TCOMM.2021.3124950, IEEE Transactions on Communications

T_{total} is inversely proportional to $\frac{v_1}{v_0}$. On the whole, when the speed of truck increases, the completion time will decrease and the efficiency will increase. To be more specific, the performance gain is significant when v_0 varies at a relatively low range (e.g., from 10 km/h to 20 km/h). While the gain obtained by accelerating the truck becomes slight when v_0 reaches a certain speed, such as 30 km/h. Similarly, when given a relatively high truck speed, the performance gain achieved by increasing the speed of UAV is also very limited. Fig. 7 indicates that the proper configuration of v_0 and v_1 is also important in practice, and it is unnecessary to blindly increase the speeds of the truck and the UAV. Also note that,

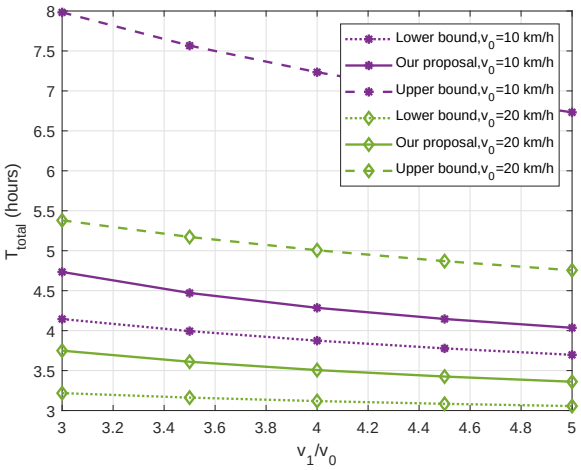

Fig. 8. Lower bound and upper bound as a function of $\frac{v_1}{v_0}$, based on the hovering positions shown in Fig. 4(f).

when given the distribution of horizontal hovering positions (i.e., given $g(x)$), the lower bound and upper bound can be calculated by (20) and (26), respectively. Here, we take uniformly distribution as an example for simplicity, and it can be seen from Fig. 8 that the total completion time of our proposal is close to the lower bound, which indicates that our proposal has substantial performance guarantee.

V. Conclusion

In this paper, we investigated the UAV-aided data collection problem in a large-scale WSN. We propose a truck carrying backup batteries to move together with a UAV so that the UAV can fly back to the truck for battery replenishment instead of flying to a fixed charging station. The optimization task of minimizing the total mission time is decomposed into two tractable proportions. First, a clustering method is developed to partition the mission region into multiple load-balanced subregions based on the prior distribution of the SNs and the capacity of the UAV, by which the horizontal positions and the altitudes of the UAV can be determined. Then, a heuristic three-step algorithm is introduced to work out the optimal rendezvous for the UAV and the truck. We give the proof of the lower and upper bounds of the proposed algorithms. Numerical results indicate that our proposal is a feasible and high-efficient way to approach large-scale data collection in practical environment. For future work, the case of multi-UAV carried by a truck may be an interesting topic.

Acknowledgement

The authors would like to thank the editors and the anonymous reviewers, whose invaluable comments helped improve the presentation of this paper substantially.

References

[1] A. Al-Fuqaha *et al.*, "Internet of Things: A Survey on enabling technologies, protocols, and applications," *IEEE Commun. Surv. Tut.*, vol. 17, no. 4, pp. 2347–2376, Fourthquarter 2015.

[2] S. L. Ullo and G. R. Sinha, "Advances in smart environment monitoring systems using IoT and sensors," *Sensors (Switzerland)*, vol. 20, no. 11, May 2020.

[3] I. Demirkol *et al.*, "Wireless sensor networks for intrusion detection: packet traffic modeling," *IEEE Commun. Lett.*, vol. 10, no. 1, pp. 22–24, Jan. 2006.

[4] S. Berrahal *et al.*, "Border surveillance monitoring using quadcopter UAV-Aided wireless sensor networks," *J. Commun. Softw. Syst.*, vol. 12, no. 1, pp. 67–82, Oct. 2016.

[5] G. Werner-Allen *et al.*, "Deploying a wireless sensor network on an active volcano," *IEEE Internet Comput.*, vol. 10, no. 2, pp. 18–25, Mar.-Apr. 2006.

[6] J. J. Estrada-López *et al.*, "Smart soil parameters estimation system using an autonomous wireless sensor network with dynamic power management strategy," *IEEE Sens. J.*, vol. 18, no. 21, pp. 8913–8923, Nov. 2018.

[7] Y. Xu, Q. Sun, and Y. Xiao, "An environmentally aware scheme of wireless sensor networks for forest fire monitoring and detection," *Future Internet*, vol. 10, no. 10, pp. 1–18, Oct. 2018.

[8] J. N. Al-Karaki and A. E. Kamal, "Routing techniques in wireless sensor networks: a survey," *IEEE Wirel. Commun.*, vol. 11, no. 6, pp. 6–28, Dec. 2004.

[9] M. Ma and Y. Yang, "Data gathering in wireless sensor networks with mobile collectors," in *Proc. IEEE IPDPS'08*, Miami, FL, USA, Apr. 2008.

[10] H. Salarian, K. W. Chin, and F. Naghdy, "An energy-efficient mobile-sink path selection strategy for wireless sensor networks," *IEEE Trans. Veh. Technol.*, vol. 63, no. 5, pp. 2407–2419, Jun. 2014.

[11] Y. Zeng, R. Zhang, and T. J. Lim, "Wireless communications with unmanned aerial vehicles: Opportunities and challenges," *IEEE Commun. Mag.*, vol. 54, no. 5, pp. 36–42, May 2016.

[12] Y. Sun, T. Wang, and S. Wang, "Location optimization and user association for unmanned aerial vehicles assisted mobile networks," *IEEE Trans. Veh. Technol.*, vol. 68, no. 10, pp. 10 056–10 065, Oct. 2019.

[13] Y. Lin, T. Wang, and S. Wang, "Trajectory planning for multi-UAV assisted wireless networks in post-disaster scenario," in *IEEE GLOBECOM'19*, Waikoloa, HI, USA, Dec. 2019.

[14] N. Hossein Motlagh, T. Taleb, and O. Arouk, "Low-altitude unmanned aerial vehicles-based Internet of Things services: Comprehensive survey and future perspectives," *IEEE Internet Things J.*, vol. 3, no. 6, pp. 899–922, Dec. 2016.

[15] S. Sotheara *et al.*, "Effective data gathering and energy efficient communication protocol in wireless sensor networks employing UAV," in *Proc. IEEE WCNC'14*, Istanbul, Turkey, Apr. 2014.

[16] A. Al-Hourani, S. Kandeepan, and A. Jamalipour, "Modeling air-to-ground path loss for low altitude platforms in urban environments," in *Proc. IEEE GLOBECOM'14*, Austin, TX, USA, Dec. 2014.

[17] C. Wang *et al.*, "Efficient aerial data collection with UAV in large-scale wireless sensor networks," *Int. J. Distrib. Sens. Netw.*, vol. 11, no. 11, Nov. 2015.

[18] J. Gong *et al.*, "Flight time minimization of UAV for data collection over wireless sensor networks," *IEEE J. Sel. Areas Commun.*, vol. 36, no. 9, pp. 1942–1954, Sept. 2018.

[19] J. Liu *et al.*, "UAV-aided data collection for information freshness in wireless sensor networks," *IEEE Trans. Wirel. Commun.*, vol. 20, no. 4, pp. 2368–2382, Apr. 2021.

[20] A. E. Abdulla *et al.*, "An optimal data collection technique for improved utility in UAS-aided networks," in *Proc. IEEE INFOCOM'14*, Toronto, ON, Canada, Apr.-May 2014, pp. 736–744.

[21] S. Say *et al.*, "Priority-based data gathering framework in UAV-assisted wireless sensor networks," *IEEE Sens. J.*, vol. 16, no. 14, pp. 5785–5794, Jul. 2016.
[22] M. Samir *et al.*, "UAV trajectory planning for data collection from time-constrained IoT devices," *IEEE Trans. Wirel. Commun.*, vol. 19, no. 1, pp. 34–46, Jan. 2020.
[23] Z. Sun *et al.*, "Two-tier communication for UAV-enabled massive IoT systems: Performance analysis and joint design of trajectory and resource allocation," *IEEE J. Sel. Areas Commun.*, vol. 39, no. 4, pp. 1132–1146, Apr. 2021.
[24] C. You and R. Zhang, "3D trajectory optimization in Rician fading for UAV-enabled data harvesting," *IEEE Trans. Wirel. Commun.*, vol. 18, no. 6, pp. 3192–3207, Jun. 2019.
[25] B. Li, Z. Fei, and Y. Zhang, "UAV communications for 5G and beyond: Recent advances and future trends," *IEEE Internet Things J.*, vol. 6, no. 2, pp. 2241–2263, Apr. 2019.
[26] K. A. Suzuki, P. Kemper Filho, and J. R. Morrison, "Automatic battery replacement system for UAVs: Analysis and design," *J. Intell. Robot. Syst.*, vol. 65, no. 1-4, pp. 563–586, Jan. 2012.
[27] X. Li *et al.*, "Rechargeable multi-UAV aided seamless coverage for QoS-guaranteed IoT networks," *IEEE Internet Things J.*, vol. 6, no. 6, pp. 10 902–10 914, Dec. 2019.
[28] S. Fu *et al.*, "Energy-efficient UAV enabled data collection via wireless charging: A reinforcement learning approach," *IEEE Internet Things J.*, vol. 8, no. 12, pp. 10 209–10 219, 2021.
[29] M. Won, "UBAT: On jointly optimizing UAV trajectories and placement of battery swap stations," in *Proc. IEEE ICRA'20*, Paris, France, May-Aug. 2020.
[30] Y. Zhu and S. Wang, "Aerial data collection with coordinated uav and truck route planning in wireless sensor network," *Proc. IEEE GLOBECOM'21, Madrid, Spain, Dec. 2021.*
[31] A. Al-Hourani, S. Kandeepan, and S. Lardner, "Optimal LAP altitude for maximum coverage," *IEEE Wirel. Commun. Lett.*, vol. 3, no. 6, pp. 569–572, Dec. 2014.
[32] Y. Zeng, J. Xu, and R. Zhang, "Energy minimization for wireless communication with rotary-wing UAV," *IEEE Trans. Wirel. Commun.*, vol. 18, no. 4, pp. 2329–2345, Apr. 2019.
[33] Y. Cai *et al.*, "Joint trajectory and resource allocation design for energy-efficient secure UAV communication systems," *IEEE Trans. Commun.*, vol. 68, no. 7, pp. 4536–4553, Jul. 2020.
[34] G. H. Ball and J. Hall, "ISODATA: a novel method of data analysis and pattern classification," Stanford Res. Inst., Stanford, CA, USA, Tech. Rep. AD-699616, 1965.
[35] J. Yang *et al.*, "An ant colony optimization method for generalized TSP problem," *Prog. Nat. Sci.*, vol. 18, no. 11, pp. 1417–1422, Nov. 2008.
[36] K. Meer, "Simulated annealing versus metropolis for a TSP instance," *Inf. Process. Lett.*, vol. 104, no. 6, pp. 216–219, Dec. 2007.
[37] S. Lin and B. W. Kernighan, "An effective heuristic algorithm for the traveling-salesman problem," *Oper. Res.*, vol. 21, no. 2, pp. 498–516, Mar.-Apr. 1973.
[38] K. Helsgaun, "General k-opt submoves for the Lin-Kernighan TSP heuristic," *Math. Program. Comput.*, vol. 1, no. 2-3, pp. 119–163, Jul. 2009.
[39] S. Boyd and L. Vandenberghe, *Convex optimization*. Cambridge, U.K.: Cambridge Univ. Press, 2004.
[40] J. G. Carlsson and S. Song, "Coordinated logistics with a truck and a drone," *Manage. Sci.*, vol. 64, no. 9, pp. 4052–4069, Sept. 2018.

Yuchao Zhu received the B.S. degree from Nanjing University, Nanjing, China, in 2020, where she is currently pursuing the Ph.D. degree with the School of Electronic Science and Engineering. Her current research interests include network planning and operations research.

Shaowei Wang (S'06-M'07-SM'13) received the PhD degree from Wuhan University, Wuhan, China, in 2006, and joined the School of Electronic Science and Engineering at Nanjing University, Nanjing, China, as a faculty member in the same year, where he is currently a Full Professor. From 2012 to 2013, he was a Visiting Scholar/Professor with Stanford University, Stanford, CA, USA, and The University of British Columbia, Vancouver, BC, Canada. His research interests include communications and networking, operations research and machine learning.